OPEN ACCESS
JOURNAL OF ADVANCED DIELECTRICS
Vol. 11, No. 3 (2021) 2140003 (10 pages)

DOI: 10.1142/S2010135X21400038

Electric, magnetic and microstructural features of the La_2CoFeO_6 lanthanide ferrocobaltite obtained by the modified Pechini route

J. A. Jaramillo Palacio[*,†], K. A. Muñoz Pulido[*,‡],
J. Arbey Rodríguez[*,‡], D. A. Landínez Téllez[*,‡]
and J. Roa-Rojas[*,§]

[*]*Grupo de Física de Nuevos Materiales, Departamento de Física*
Universidad Nacional de Colombia, Bogotá DC, Colombia

[†]*Laboratório de Magnetismo e Materiais Magnéticos*
Departamento de Física, Universidade Federal de Santa Maria
Rio Grande do Sul Brazil

[‡]*Grupo de Estudios de Materiales, Departamento de Física*
Universidad Nacional de Colombia, Bogotá DC, Colombia

[§]jroar@unal.edu.co

Received 17 January 2021; Revised 27 March 2021; Accepted 19 April 2021; Published 11 June 2021

In the search for new materials with applicable magnetic properties in spintronic devices, the aim of this work is to report the synthesis of the lanthanide ferrocobaltite La_2CoFeO_6 using the modified Pechini route; the experimental study of structural, morphological and magnetic properties, and the analysis of the electronic structure and bands are obtained in the framework of the Density Functional Theory. Rietveld refinement of experimental X-ray diffraction patterns revealed the crystallization of this oxide material in a perovskite-like monoclinic structure, space group $P2_1/n$ (# 14). Scanning electron microscopy and atomic force microscopy images revealed that the surface morphology is essentially polycrystalline, with mean grain sizes between 177 and 188 nm. The dispersive X-ray spectroscopy suggests that the material obtained contains La, Fe, Co and O in the stoichiometric proportions expected by up to 98%. The magnetic susceptibility curves as a function of temperature indicated that the material is ordered ferromagnetically, showing strong irreversibility effects due to the disorder of the Fe and Co cations in the three crystallographic directions of the structure and to the strong distortions in the FeO_6 and CoO_6 octahedra. Magnetic hysteresis curves confirmed the ferromagnetic character of the material for all temperatures evaluated, up to room temperature. I–V response curves revealed a semiconductor-like behavior with a figure of merit exponent 1.53 of the varistor type. The ferromagnetic semiconductor behavior suggests the potential applicability of the material in spintronic technological devices.

Keywords: Double perovskite; Pechini method; crystalline structure; ferromagnetic response; semiconductor behavior.

1. Introduction

Perovskites are materials, which generally form cubic structures, exhibit behavior from insulators to superconductors, through semiconductors, metal conductors, manganites and ferroelectric.[1] The alteration of the ideal structure of perovskites gives rise to the possibility of finding new electrical and magnetic properties. In their ideal form, perovskites are described by the generalized expression ABX_3, consist of cubes composed of three different chemical elements A, B and X present in a 1: 1: 3 ratio and have cubic structure. Atoms A and B are metal cations (positively charged ions) and X sites correspond to nonmetallic anions (negatively charged ions) that are usually occupied by oxygen or halogen elements. Structurally, cation B is sited in the center of the cube, cation A that has the largest atomic radius occupies the eight vertices and X-anions are centered on the faces of the cubic cell.[2] The perovskite structure is susceptible to variations in the A and B cations. One of the most usual modifications allows obtaining the known double perovskite $A_2BB'O_6$, where 50% of the sites of the metal cation B are replaced by another transition metal B′.[3] When cations B and B' alternate along the crystallographic axes throughout the structure, it is said that there is cationic ordering, forming a superstructure.[4] In principle, the factors that control the arrangement of the B cations within the structure are ionic radii, oxidation state, ionization potentials of both and ratio of the size of the A/B and A/B′ cations. Of the above, the most influential factor is related to the oxidation states that establish the boundary between a rock-salt structure (superstructure), and one without ordering.[5] In an ideal cubic structure, the unit

[§]Corresponding author.

cell has no adjustable position parameters, giving rise to a change of the lattice parameter when the composition of the material is modified (in an approximation in which the atoms touch each other). In the case of a distorted perovskite, the length of the A–O bond is $\sqrt{2}$ times less than the length of the B–O and B′–O bonds.[6] This effect can be quantified by means of the Goldschmidt tolerance factor, which establishes a simple relationship between the interatomic distances A–O, B–O and B′–O, assuming that the structure of a perovskite is ionic and that each atom has a corresponding average ionic radius that allows them to be in contact with each other. The tolerance factor for the $A_2BB'O_6$ double perovskite is set as follows[6]:

$$\tau = \frac{\sqrt{2}(r_A + r_O)}{(r_B + r_{B'} + 2r_O)} \quad (1)$$

where r_A, r_B and $r_{B'}$ are the ionic radii of the A, B and B′ cations and r_O represents the ionic radius of the anion O. In addition to these characteristics, the octahedral coordination of cations B and B′ with the oxygen anions, forming the B-O_6 and B′-O_6, structures, undergo distortions that depend on the ionic radii,[7] as well as the electrical[8] or magnetic character[9] of the cations and its interaction with neighboring cations. In this way, the new or exotic electrical and magnetic properties in materials of the perovskite family have their origin in the dimensions and in the electronic characteristics of the cations A, B and B′, and, of course, are closely related with the structural distortions of the crystallographic cell of the material. Ferrites and cobaltites of lanthanide elements have been studied for many years.

Particularly, Lanthanum cobaltite $LaCoO_3$ was studied by Jonker and van Santen in 1953[10] very shortly after reporting Lanthanum Manganite[11,12] famous in the 90's for the colossal magnetoresistive behavior.[13] One of the most interesting results initially observed in this material has to do with its total effective magnetic moment, whose value is greater than that expected from the electronic spin moments of Co^{3+} in the high-spin configuration.[10] Five years later, explanations based on the contributions were suggested, which are due to the occurrence of Co^{3+} ions are in the structure at octahedrally coordinated sites under a strong crystalline field intensity,[14] and 12 years later, contributions of spin-orbit effects were included, not forgetting that at that time, the structure of the perovskites was expected to be cubic with probably trigonal distortions.[15] The electrical and magnetic properties, as well as the different possible interactions, including coexistence of low-spin and high-spin configurations of Co cation were analyzed in the 60s and 70s.[16,17] Its exotic properties were theoretically analyzed from calculations of electronic structure, considering several possible spin configurations, with proposals for the occurrence of a transition between a low-spin configuration and an intermediate-spin state[18] and not long ago, it analyzed the effect of synthesis techniques on the physical properties of the material.[19]

On the other hand, $LaFeO_3$ lanthanum orthoferrite has been extensively studied since its first reports in the 50's, due to its G-type antiferromagnetic properties,[20] exchange-bias,[21] its simultaneously ferroelectric (multiferroic) feature[22] and weak ferromagnetism.[23] Meanwhile, some results suggest that the robustness of the ferromagnetic and ferroelectric responses in this material depend on the synthesis conditions.[24]

Despite the apparent similarity in the chemical formula of these two perovskite-type materials, $LaCoO_3$ lanthanum cobaltite crystallizes in a rhombohedral structure, belonging to the R-3c (# 167) space group, with tolerance factor $t = 1.012$ and distortions in lag for the three octahedral subaxes according to Glazer $a^-a^-a^-$ notation, while the $LaFeO_3$ lanthanum orthoferrite adopts an orthorhombic crystalline structure, belonging to the Pnmb space group (# 62), with tolerance factor $t = 0.951$ and octahedral distortions given by $a^+b^-b^-$. These substantial differences, in addition to the magnetic implications due to the crystalline field and the intrinsic characteristics of the Co^{3+} and Fe^{3+} cations, have direct inference about the exotic physical properties than these exhibits. Because of the above information, it is interesting to study a complex perovskite type material that results from the union of these two simple perovskites: $LaCoO_3 + LaFeO_3 = La_2CoFeO_6$. Some theoretical studies, considering tetragonal, monoclinic and rhombohedral structures of La_2CoFeO_6, predict that this material should behave like a ferromagnetic semiconductor.[25,26] Recently, the magnetic and dielectric properties of La_2CoFeO_6 samples prepared by means of the co-precipitation technique were studied.[27] However, the obtaining of a pure crystallographic phase is not reported, since a mixture of rhombohedral and monoclinic structures belonging to the R-3 (# 148) and $P2_1/n$ (# 14) space groups was obtained, whose disorder has influence on the physical properties analyzed.[27] Meanwhile, there are not enough reports on the experimental obtaining of a single crystallographic phase for this material. Therefore, in order to contribute to the clarification of the behaviors exhibited by this material, in this paper, the synthesis process of the perovskite La_2CoFeO_6 through the modified Pechini method and structural, morphological, magnetic and electric characterization are reported.

2. Experimental Setup

The La_2CoFeO_6 sample was synthesized following the modified Pechini method, within which La_2O_3 (Aldrich 99.9%) was previously dissolved in water together with HNO_3 65%, adding to it $Fe(NO_3)_3$; $9H_2O$ (Aldrich 99.9%) and $Co(NO_3)_2$; $5H_2O$ (Aldrich 99.99%) to a solution of $C_6H_8O_7$ (Aldrich 99%) whose function during the process was to play the role of chelating agent (CA). This CA was dissolved in water, adhered in a ratio of 1:1 CA (metal molar ratio) to promote the formation of a complex. Ethylene Glycol (EA) was included in this solution in a 1:2 CA–EA ratio to act as an esterifying

agent, with the function of synthesizing an ester and promoting the formation of a polymeric lattice. Subsequently, the obtained product was subjected to a slow evaporation of water at $T = 100\,°C$ to form the polymeric lattice, over a time of 15 h, under constant magnetic stirring. Once the polymerization was obtained, the mixture was grinded and pressed in eight samples with cylindrical form, which were submitted to sintering processes for 1 h at different temperatures (*TS*) of 500, 550, 600, 650, 700, 800, 900 and 1000 °C. The study of the crystal structure was carried out by means of X-ray diffraction experiments, using a Panalytical X-Pert PRO MPD diffractometer with $\lambda_{CuK\alpha} = 1.540598\ Å$. Analysis of the experimental diffraction patterns was performed using Rietveld refinement procedures through the GSAS+EXPGUI code,[28–30] obtaining information on the structural parameters and the corresponding spatial group. The morphology of the sample was examined using a VEGA3 Tescan scanning electron microscope (SEM) and a Park System NX10 atomic force microscope (AFM) in tapping mode with a selected frequency $\nu = 282.7$ kHz. The semi-quantitative comparison of the nominal stoichiometry of the sample was obtained by means of X-ray dispersive energy (EDS) experiments, using a Bruker X-ray gun coupled to the SEM. The magnetic behavior of the sample was observed through a vibrating sample magnetometer Cryogenic VSM 5T system. The temperature susceptibility was measured in the range $50\ K < T < 300\ K$ on the application of external fields of 500, 2000 and 10000 Oe, following the Zero Field Cooling (ZFC) and Field Cooled (FC) procedures.[31] Curves of magnetization as a function of applied fields up to ±45 kOe were obtained for temperatures of 25, 50, 100, 200 and 300 K. Current–Voltage (I–V) electrical response curves at room temperature ($T = 300$ K) were measured using a Keithley-6517A Direct Current electrometer, whose sample holder contains gold-plated silver contacts.

3. Results and Discussion

3.1. *Crystallographic and microstructural characteristics*

As part of the synthesis process, eight samples from the same batch of the Pechini recipe described in Sec. 2 were selected. These eight samples were subjected to different and independent sintering temperatures *TS* of 500, 550, 600, 650, 700, 800, 900 and 1000 °C, respectively, so that each of them was subjected to X-ray diffraction experiments. In Fig. 1, the diffraction patterns obtained for the sintering temperatures of different samples of La_2CoFeO_6 after a joint polymerization process are presented sequentially.

As can be seen in Fig. 1, at sintering temperatures close to 1000 °C the material already tends to show a single crystalline phase. For sintering at $T = 550\,°C$, it is possible to note the occurrence of a majority crystalline phase.

However, as the sintering temperature increases, a systematic decrease in the width of the diffraction peaks is observed, which is related to the increase in the average size of the

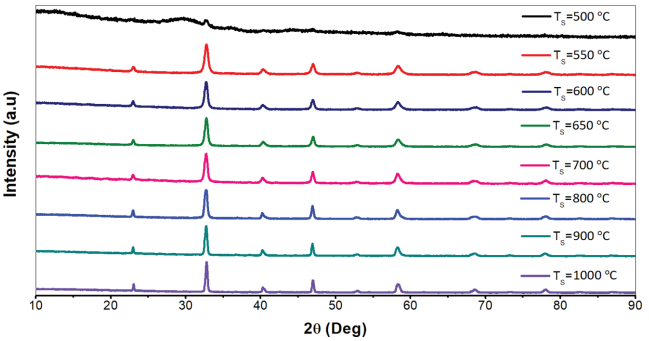

Fig. 1. Diffractograms obtained for samples submitted to different sintering temperatures after applying the modified Pechini technique.

crystallite. The experimental crystallite size D was calculated from the Scherrer equation[32] for the diffraction patterns shown in Fig. 1, in the sintering temperature regime $650\,°C < T_S < 1000\,°C$. The value of D is based on the widening of the peak intensity peak of the XRD pattern due exclusively to the particle size and is defined by the ratio

$$D_{hkl} = \frac{\kappa\lambda}{W\cos\theta}, \tag{2}$$

where D_{hkl} represents the size of the crystallite and only depends on the *hkl* directions, κ is a dimensionless shape factor with typical value 0.9, $\lambda = 1.54056$ Å is the wavelength applied in the XRD experiment, W is the average width in half of the diffraction peak and θ is the Bragg angle.

The dislocation density, as a measure of the number of defects in the samples is given by[32] $\delta = \frac{1}{D^2}$ and the lattice strain induced in powder samples due to crystal imperfection and distortions was calculated from the following equation[33]:

$$\varepsilon = \frac{\kappa\lambda}{4D_{hkl}\sin\theta}, \tag{3}$$

The obtained mean crystallite sizes, dislocation densities and lattice strains are shown in Table 1.

It can be intuited from the data in Table 1 that the sintering process at higher temperatures leads to a substantial

Table 1. Mean crystallite sizes for different sintering temperatures.

T_S (°C)	D_{hkl} (nm)	δ ($\times 10^{-4}$/nm^2)	ε (%)
650	29.5	11.5	29.40
700	31.7	10.6	28.66
800	43.5	5.3	25.75
900	52.3	3.7	23.20
1000	60.8	2.7	20.81

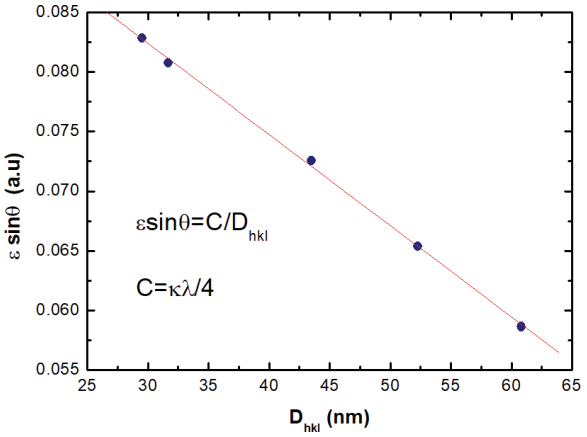

Fig. 2. Lattice strain as a function of crystallite size for samples sintered at different temperatures according with Table 1.

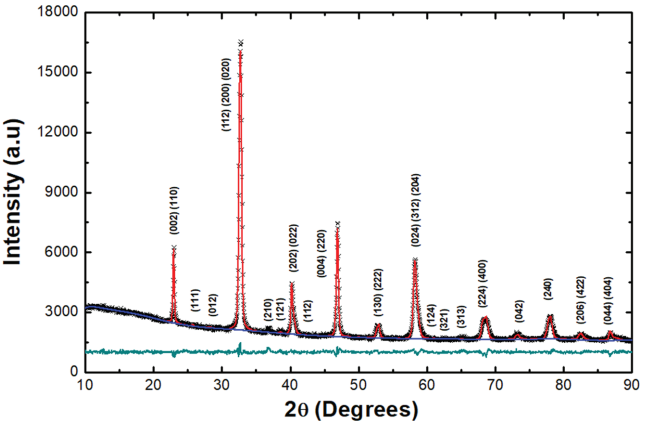

Fig. 3. Refined XRD pattern for the sample sintered at T = 1000 °C.

increase in the crystallite size, decreasing the number of defects in the samples, represented in the dislocation density. Similarly, the $\varepsilon \sin\theta$ decreases with a linear trend as the crystallite size increases, as seen in Fig. 2, because the sintering process densifies the samples by means of interdiffusion between the grains and the increase in both the grains and the crystals that make them up, making the presence of defects and the stresses due to their occurrence less likely. The presence of all these types of defects in the crystalline material locally modifies the structural periodic order, substantially affecting the properties of electrical transport, since the dislocations change the orientation of the crystallites, generating centers of dispersion in the transport of charge carriers, also giving rise to the occurrence of electrical polarization effects. The impact of defects on the electrical response will be discussed in Sec. 3.4 of this paper.

Once the presence of a majority phase close to 99.5% in the sintered sample at 1000 °C was established, the refined diffraction pattern by using the GSAS II code[28] for the La_2FeCoO_6 material is exemplified in Fig. 1 for this sintering temperature. The main reliability parameters of refinement were $\chi^2 = 1.251$ and $F^2 = 4.21\%$, whose values suggest a high-quality Rietveld analysis, which can be seen in Fig. 3 through the good correspondence between the theoretical diffraction pattern and the experimental diffractogram.

The best fit between simulated data and data from the diffractometer corresponds to a perovskite monoclinic structure belonging to the $P2_1/n$ (# 14) space group, as has been theoretically predicted,[26] and far from the reported monoclinic and rombohedral phase mixture for this material obtained by the co-precipitation method.[27] The notation of this spatial group corresponds to a primitive structure with a rotation of 180° of order two around a screw-type axis followed by a translation of half a cell parameter in the [010] direction, and with a sliding reflection plane perpendicular to the direction [010].

From the structural analysis the cell parameters a = 5.4672 Å, b = 5.5058 Å and c = 7.7503 Å were obtained, with the monoclinic angle $\beta = 90.1215°$. Table 2 presents a complete scheme of the atomic positions and bond distances that resulted from the Rietveld refinement.

In Table 1, the notation b, d and e, known as Wyckoff letters, determine all x points for which the symmetry groups at each site in the cell are conjugated subgroups of the space group $P2_1/n$.[34] These letters constitute only a coding framework for Wyckoff's positions, beginning with one at the bottom position and continuing in alphabetical order.[35] The number of equivalent dots per unit cell that accompanies Wyckoff's letter is known as the multiplicity of Wyckoff's position. The results shown in Table 1 reveal the distorted character of the unit cell for the La_2FeCoO_6 double perovskite type material. In particular, the out-of-equilibrium

Table 2. Crystallographic distances and angles obtained from the Rietveld refinement.

Wyckoff	La	Fe	Co	O(1)	O(2)	O(3)
site	4e	2d	2b	4e	4e	4e
x (Å)	0.0000	0.0000	0.5000	0.2801	0.2311	0.3821
y (Å)	0.0000	0.5000	0.0000	0.2612	0.7803	–0.0060
z (Å)	0.2500	0.0000	0.0000	0.0270	0.0270	0.0250

Octahedral main inter-atomic distances and valences

Cation	Anion	Distance (Å)	Valence	Main bond angles	Degrees (°)
Fe	O(1)	2.0107	0.5000	Fe–O(1)–Co	162.8
Fe	O(2)	2.0187	0.4999	Fe–O(2)–Co	162.7
Fe	O(3)	2.0250	0.5001	Fe–O(3)–Co	162.7
Co	O(1)	1.8893	0.5000	Octahedral tilt angles	Degrees (°)
Co	O(2)	1.8963	0.4999	ρ (2d)	9.020
Co	O(3)	1.9020	0.5001	η (2b)	9.607

positions of the anions in the unit cell are a first indication of the distorting trend of the FeO_6 and CoO_6 octahedra. Other evidence of the tilting nature of octahedra is in the differences in the inter-atomic distances of the Fe and Co cations with respect to the anions O(1), O(2) and O(3), in addition to the appearance of angles in the Fe–O–Co bonds other than 180°, as well as the occurrence of angles ρ and η different from zero degrees. Finally, the deviation of the structure from the cell of an ideal cubic perovskite is given by the tolerance factor (Eq. (1)), that for the La_2FeCoO_6 material is τ = 0.9780, which indicates a deviation greater than 2% of the unit cell with respect to a perfect cubic for which τ = 1 is expected. This distortive tendency of the structure is related to the differences between the ionic radii of the constituent atoms of the material, which together with the eventual electronic correlations, as well as to the crystalline field effects due to the presence of *3d* orbitals in the octahedra, causes rotations and tilts that influence the magnetic response of the material. In Glazer's notation for octahedral distortions,[36] this structure corresponds to the system denoted $a^-b^+a^-$. In this notation, superscript (0) represents no tilt around an axis, (+) in-phase tilt and (-) out-of-phase tilt, which means that in the La_2FeCoO_6 material the octahedrons rotate out-of-phase along of the crystallographic axes *a* and *c* in-phase along the *b* axis. The occurrence of reflections indexed as (004), (204) and (404) are directly related with the octahedral in-phase tilting (*ood*) along the direction of the *b* cell parameter. These effects are easily observed in the crystal structure shown in Fig. 4(a).

As seen in Fig. 4(b), while FeO_6 octahedra elongate axially, CoO_6 octahedra elongate equatorially, introducing asymmetries that can influence the magnetic response. These differences in the local environment (shape and size) of the octahedra could force the appearance of canted magnetic moments, which give rise to magnetic anisotropy effects.

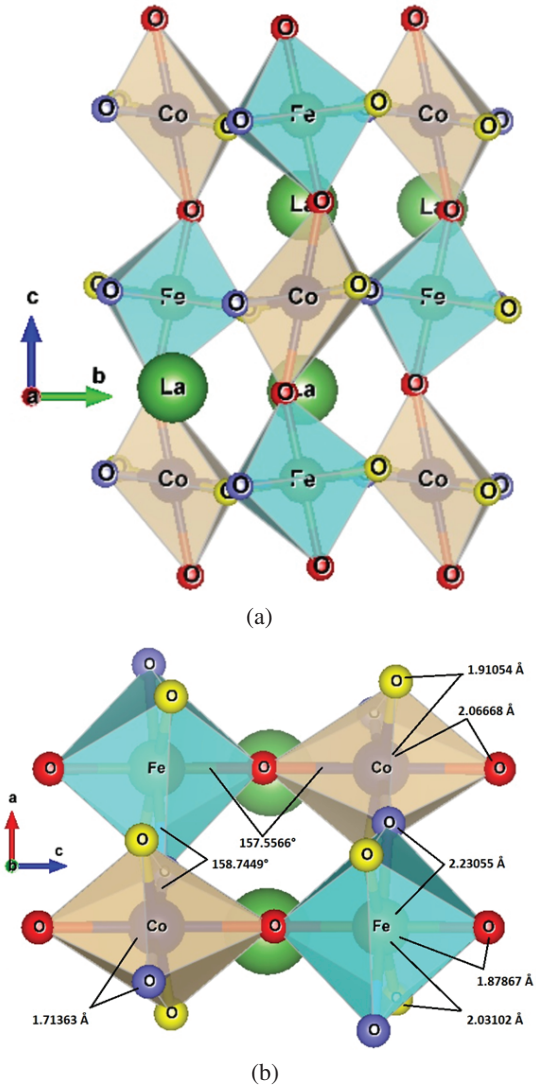

Fig. 4. Structure of the La_2FeCoO_6 in the $P2_1/n$ (#14) space group. In-phase tilting along the *b*-axis and out-of-phase along the *c*-axis is observed in figure (a). Bond inter-atomic distances and angles are shown in figure (b).

3.2. *Surface morphology and composition*

A first approximation to the surface morphology of La_2CoFeO_6 was carried out through SEM images from secondary electrons under the application of 9 kV and a magnification of 35 kX, as exemplified in Fig. 5. In the image, an essentially polycrystalline distribution is observed, which is formed by grains of random sizes and shapes, with cavities of submicron dimensions in the intergranular interstices, evidencing the porous character of the surface. The largest

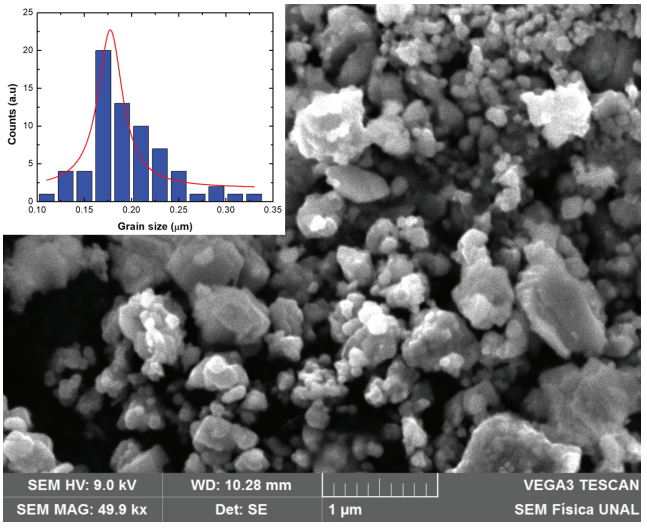

Fig. 5. SEM image of secondary electrons on a representative surface region for the La_2FeCoO_6 sample sintered at T_S = 1000 °C. The inset corresponds to the grain size analysis obtained from the ImageJ software application.[37]

grains are since the sample under analysis corresponds to T_S = 1000 °C, so one of the effects of this higher sintering temperature was the growth of some grains above the volumetric average of the material.

Furthermore, the micrograph shows that some of the more superficial grains were charged due to the large potential difference and the probable semiconductor character of the material,[26] acquiring a brighter appearance than those less superficial grains. The inset of Fig. 5 shows the analysis of the grain size from the use of the ImageJ,[37] which is based on the known intercept method. Using this technique, the mean size obtained for the surface grains was 177 ± 25 nm.

A second analysis of the surface topography of the La_2FeCoO_6 material was carried out using images from AFM microscopy. The corresponding image is exemplified in Fig. 6(a) for the sample sintered at T_S = 1000 °C. The analysis for grain size from the AFM surface image is represented in Fig. 6(b). This provides an average grain size value of 188 ± 19 nm, which is 94% in accordance with the analysis from SEM images. As will be seen later, the nanometric order in the average granular size will have relevance in the analysis of the magnetic response of the material.

The semiquantitative analysis of the composition was performed using a Bruker X-ray cannon coupled to the VEGA3 TESCAN scanning electron microscope, thereby obtaining the EDS spectrum shown in Fig. 7.

In Fig. 7, the spectral peaks obtained are due to transitions between orbitals corresponding only to the atoms of La, Fe, Co and O, without the presence of impurities acquired during the synthesis process. The weight percentage of each of the components of the La_2FeCoO_6 material is obtained through the deconvolution of the curve formed by the energy spectrum. As observed in Table 3, the experimental values obtained from the area under the curve in Fig. 7 are 98% in agreement with those calculated from the stoichiometry given by the chemical formula of the sample. It is observed in Table 3 that there is a greater difference between the experimental and theoretical values in the case of oxygen due to its relatively small mass compared to the masses of the other atoms in the sample, so its efficiency in X-ray beam scattering is less than those of La, Fe and Co.

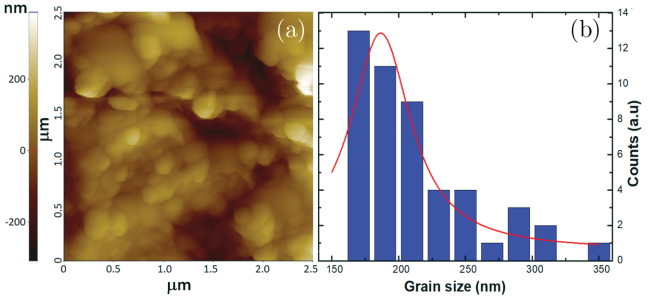

Fig. 6. AFM image for the La_2FeCoO_6 sample sintered at T_S = 1000 °C (a), and analysis of the grain size obtained from the AFM micrograph (b).

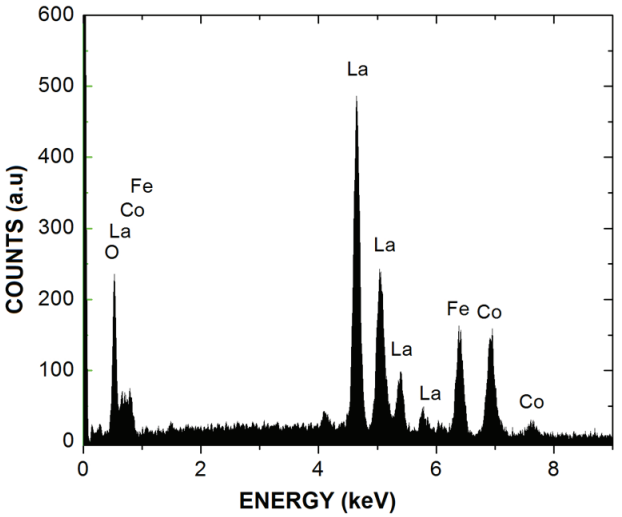

Fig. 7. EDS spectrum analyzed to obtain composition for the La_2FeCoO_6 double perovskite sintered at T_S = 1000 °C.

Table 3. Comparison between the experimental and stoichiometric weight percentages for each of the components of the La_2FeCoO_6 material.

Atom	Exp. W%	Stoich. W%
La	55.62	56.86
Fe	11.07	11.42
Co	12.03	12.06
O	21.28	19.64

3.3. *Magnetic response*

Magnetic susceptibility measurements as a function of temperature were carried out under the application of H magnetic fields of 500, 2000 and 10,000 Oe, with the aim of experimentally analyzing the magnetic response of this interesting material. In all three cases, the susceptibility behaviors were evaluated, considering the recipes ZFC and FC shown in Fig. 8.

The information provided by the susceptibility curves in Fig. 8 is varied. First, it is clearly seen that at T = 320 K, for all the applied magnetic field strengths, there is a finite susceptibility related to the occurrence of ordering of magnetic moments. Secondly, the ZFC and FC curves present different trajectories, evidencing the existence of irreversibility. In the meantime, it was not possible to establish the value of the irreversibility temperature because it takes place for temperature values greater than the maximum temperature

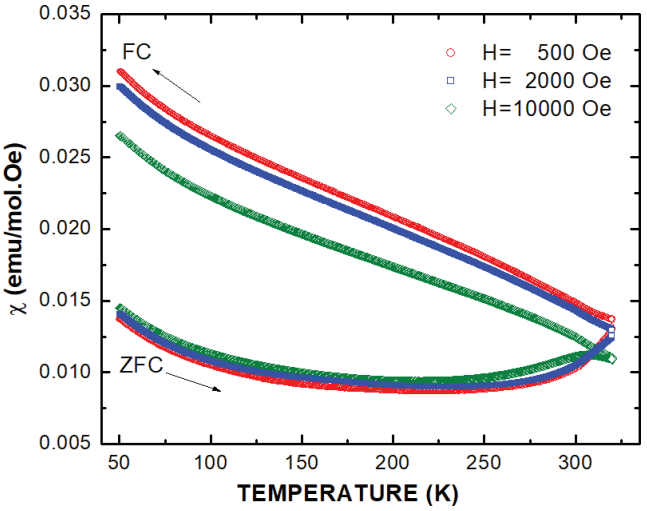

Fig. 8. Magnetic susceptibility as a function of temperature for the La_2CoFeO_6 complex perovskite sintered at $T_S = 1000\,°C$.

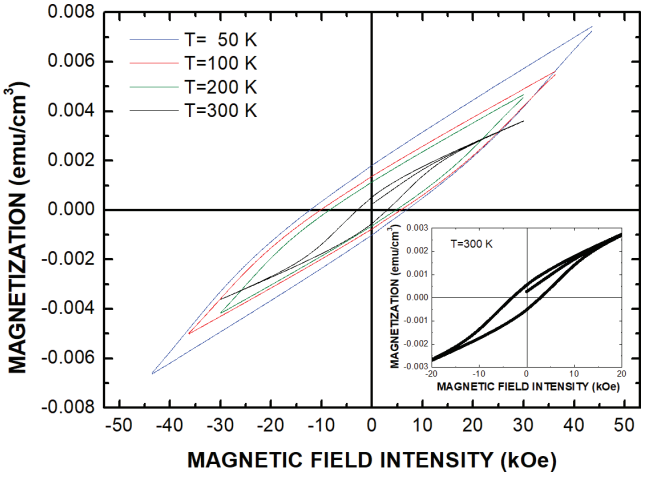

Fig. 9. Isothermal magnetic hysteresis curves for the La_2CoFeO_6 material sintered at $T_S = 1000\,°C$. The inset corresponds to a close-up of the hysteresis curve at room temperature.

measured in this experiment (320 K), suggesting that the type of arrangement is ferromagnetic. The irreversible behavior is determined by the effects of disorder that cause a spin-glass type response in the magnetic moments of the system at low temperatures. In perovskite-like materials, the majority responsible for the irreversible response is the disorder of the magnetic cations in the crystalline structure, in this case, the Fe and Co cations. In other words, the nonformation of a superstructure where the FeO_6 and CoO_6 octahedra are distributed alternately along the crystallographic axes causes the breakdown of the correlation between ferromagnetic domains that characterizes ordered ferromagnetic materials, so that ferromagnetism remains in the material but the lack of correlation between domains causes the difference between the ZFC and FC responses in the magnetic susceptibility.

A further contribution to the irreversible character has to do with the crystalline anisotropy caused by the octahedral tilting of the FeO_6 and CoO_6 in-phase along the crystallographic *y* direction and out-of-phase in the *x*- and *z*- directions, which introduces the blocking of the magnetic domains at low temperatures, making it difficult to align moments with the applied field during the ZFC procedure. When starting the ZFC recipe, at low temperatures, the curve exhibits a slight decrease with increasing temperature up to $T = 200$ K, where the susceptibility increases, presumably up to the value of the irreversibility temperature. Meanwhile, when the FC procedure is started, decreasing the temperature in the presence of an external field, the susceptibility increases, showing that the system is ferromagnetic but there are still domains to be aligned. Upon reaching the minimum measurement temperature value (50 K), saturation has not yet been reached for any of the applied field intensities. For this reason, it was not possible to determine the value of the effective magnetic moment using this measurement technique. On the other hand, the differences in shapes and sizes, as well as the interatomic distances and the bond angles observed between the FeO_6 and CoO_6 octahedra, influence the exchange potentials between the magnetic moments due to the Fe and Co cations. This characteristic includes canting effects on the magnetic spins that magnify the nature of the disorder, giving rise to a marked irreversible response as seen in the magnetic susceptibility curves ZFC and FC in Fig. 8.

Figure 9 represents systematic measurements of magnetization as a function of the applied field were carried out at temperature values 25, 50, 100, 200 and 300 K on the application of external fields up to ±45 kOe. As expected from the magnetic susceptibility results, there is a decrease in the number of aligned magnetic domains due to the increase in temperature, which occurs because the increase in entropy decreases the effective exchange energy that characterizes ferromagnetic feature. For this reason, with the increase in temperature, not only does magnetization decrease, but the area enclosed in the hysteresis curve decreases, since it represents the magnetic energy of the system. Consequently, the characteristic magnetic parameters change proportionally, as detailed in Table 4, where the decreasing behavior of the coercive field (*HC*) values and the remnant (*MR*) magnetization is observed.

Table 4. Temperature dependence of the magnetic parameters in the La_2FeCoO_6 material.

Temperature (K)	H_C (Oe)	M_R (emu/cm^3)
50	7500	0.00175
100	5460	0.00138
200	4550	0.00114
300	3050	0.00052

The coercive field values presented in Table 4 are much higher than those reported for the lanthanide orthoferrite[38] $LaFeO_3$ and correspond to about half of those H_C values for $La_{1-x}Bi_xFeO_3$,[39] which is an indication of the robustness of the ferromagnetic response in the La_2FeCoO_6 double perovskite, even at room temperature, as can be seen in the inset of Fig. 9. This hysteresis curve starts at a nonzero magnetization value because the sample was magnetized due to measurements at lower temperatures. As observed in Table 4, the remnant magnetization values are moderate for the evaluated temperature values. Meanwhile, under the application of field strengths of up to 45 kOe, saturation magnetization was not reached, so it is expected that under the application of much higher fields, its value will increase and the hysteresis curve will become more robust, so the magnetic parameters could allow the material to be classified as hard ferromagnetic.

The type of magnetic coupling that gives rise to the mainly ferromagnetic response of the La_2FeCoO_6 material differs substantially from the superexchange interaction that confers antiferromagnetic characteristics to $LaFeO_3$,[23] as well as from the spin-orbit effects that strongly modify the crystalline field to produce antiferromagnetism in $LaCoO_3$.[19] A reasonable model is based on the third Goodenough–Kanamori–Anderson (GKA) rule, according to which an overlap half-fill and empty 180° exchange is expected to produce a weak ferromagnetic response in this type of structure.[40] Although our material reveals Fe–O–Co bonds with angles around 159°, this angular difference does not prevent the occurrence of a potential due to two-center two-electron exchange interactions that they give rise to spin-polarization, with jumps favoring a ferromagnetic alignment of magnetic moments in the same unoccupied orbital site, orienting the spins to give rise to a robust ferromagnetic intra-site exchange. Specifically, this exchange would take place between the electrons of the high-spin ($d_{x^2-z^2}$) orbitals of Fe with the high-spin (d_{x^2}) orbitals of Co mediated by the *Px* orbitals of Oxygen. The spin-polarization is one of the reasons why the material becomes semiconductor (as we will see in the next section), in contrast to the dielectric character exhibited by the lanthanide ferrite $LaFeO_3$[41] and the Lanthanum cobaltite $LaCoO_3$.[42]

3.4. *I–V characteristic curve*

With the aim to analyze the behavior of the electrical response of the material at room temperature, measurements of the I–V response were carried out on the La_2FeCoO_6 material. The result obtained is shown in Fig. 10 for applied voltages between −400 V and 400 V.

As seen in Fig. 10, the change in voltage causes a nonlinear variation of the current in the material, with a tendency towards a varistor-like behavior.[43] The current increases following a power law with increasing voltage, of type

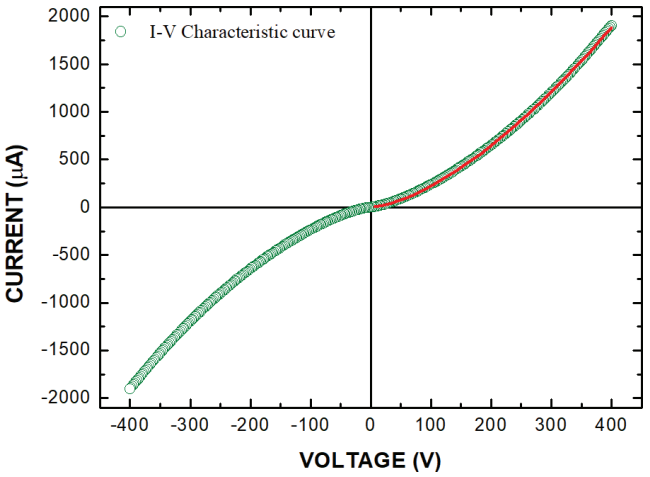

Fig. 10. I–V characteristic curve measured for the La_2CoFeO_6 complex perovskite.

$I = I_o V^{\beta}$. Initially, the increase in voltage induces small currents due to the occurrence of polarization effects, and mixtures between dielectric responses and granular boundary relaxation effects. Subsequently, the electrons promoted through the gap from the valence band of the semiconductor lead, tending to linearize the behavior of the I–V curve for high applied voltages. The values of the constant and the exponent in the power law tend to $I_o = 0.19$ μA and $\beta \approx 1.53$. Implicit in this behavior is the additional thermal response that deviates the electrical response behavior from Ohm's law. Thus, it is possible to expect a dissipation power that grows rapidly with voltage ($P \sim V^{\beta+1}$). This dissipation has to do with the occurrence of Schottky barriers formed by grain boundaries, which gives rise to a nonlinear characteristic of the I–V curve observed in Fig. 10.[44] These barriers are made up of micro-junctions where a pair of grains can be seen as two consecutive Zener diodes. Thus, the intergranular boundaries along the material behave as resistors that produce currents like those expected in a varistor diode. For high voltage values, the resistance follows the expected Ohmic trend, but in this regime, the resistivity decreases because the intragranular contributions are more relevant than the intergranular ones. In this way, microstructural electrical transport can be modeled through equivalent electrical circuits that are related to intra- and inter-granular transport currents within the material.[45] According to this model, the figure of merit I–V of the varistor has the form of a power law, like the one mentioned above, where I_o is a free constant and β is the nonlinear coefficient, whose value close to 3/2 is predicted by the quasi-hydrodynamic semiconductor equations and was attributed to regions of sample with vanishing carriers.[46,47] The ferromagnetic semiconductor character established from the experimental results is in accordance with the theoretical predictions made for La_2FeCoO_6 material through electronic structure calculations.[25,26]

4. Conclusions

Samples of La_2FeCoO_6 were produced by the modified Pechini method. The structural analysis shows that this technique allows the crystallization of the material in a single phase of the monoclinic perovskite type, space group $P2_1/n$ with strong distortions in the FeO_6 and CoO_6 octahedral coordinations. The microstructural analysis showed the occurrence of dislocations and defects, which affects the electrical transport mechanisms of the material. The density of dislocations and defects is sensitive to the optimization of the heat treatments applied during the material synthesis process. SEM and AFM images made it possible to establish the essentially granular character of the material surface, with grain sizes of nanometric dimensions. The compositional study revealed that the material produced contains 98% of the expected composition from its stoichiometric formula. Measurements of DC magnetization as a function of temperature and the applied magnetic field showed the ferromagnetic character of the material, with irreversibility effects related to the disorder produced by the structural distortions and microstructural anomalies of the material. Curves of I–V response suggest the occurrence of a varistor-type semiconductor electrical transport characteristic, following a figure of merit predicted by the quasi-hydrodynamic semiconductor model. The ferromagnetic and semiconductor characteristics observed in the La_2FeCoO_6 double perovskite allow proposing possible applications in technologies that involve the manipulation of electronic spin (spintronics) for the design of semiconductor devices with modulation of the magnetic response by controlling the properties of electric charge transport, for the production of magnetic sensors, mechanisms for storage and reading of random access information and spin transistors, with a particular advantage: the occurrence of the ferromagnetic property and the semiconductor response in a single material.

Acknowledgments

This work was partially supported by Division of Investigation and Extension (DIEB) of the National University of Colombia, Hermes code 48069, MINCIENCIAS on the project FP80740-243-2019 and Coordenação de Aperfeiçoamento de Pessoal de Nível Superior — Brasil (CAPES) — Finance Code 001. A special thanks to Dr. Julio C. Denardim for facilitating his laboratory equipment at the University of Santiago, Chile.

References

[1]N. W. Thomas, Crystal structure–physical property relationships in perovskites, *Acta Cryst.* **B45**, 337 (1989).
[2]R. M. Hazen, Perovskites*, Sci. Am*. **258**, 52 (1988).
[3]C. A. Triana, D. A. Landínez Téllez and J. Roa-Rojas, Synthesis process and structural characterization of the Sr_2EuRuO_6 complex perovskite, *J. Alloys Compd*. **516**, 179 (2012).
[4]J. A. Grisales Cerón, J. Arbey Rodríguez, A. Rosales-Rivera, N. A. Salazar, H. J. A. Cuervo Farfán, J. A. Cardona Vasquez, D. A. Landínez Téllez and J. Roa-Rojas, Mott insulator behavior in the yttrium-based antimoniate oxide Ba_2YSbO_6, *J. Mater. Res. Technol*. **8**, 3978 (2019).
[5]G. King and P. M. Woodward, Cation ordering in perovskites, *J. Mater. Chem*. **20**, 5785 (2010).
[6]V. M. Goldschmidt, Die Gesetze der Krystallochemie. *Naturwissenschaften* **14**, 477 (1926).
[7]P. M. Woodward, Octahedral tilting in perovskites. I. Geometrical considerations, *Acta Cryst.* **B53**, 32 (1997).
[8]K. S. Aleksandrov, Mechanisms of the ferroelectric and structural phase transitions. structural distortions in perovskites, *Ferroelectrics* **20**, 61 (2011).
[9]M. W. Lufaso and P. M. Woodward, Jahn–Teller distortions, cation ordering and octahedral tilting in perovskites, *Acta Cryst.* **B60**, 10 (2004).
[10]G. H. Jonker and J. H. Van Santen, Magnetic compounds wtth perovskite structure III. ferromagnetic compounds of cobalt, *Physica* **19**, 120 (1953).
[11]G. H. Jonker and J. H. Van Santen, Ferromagnetic compounds of manganese with perovskite structure, *Physica* **16**, 337 (1950).
[12]J. H. Van Santen and G. H. Jonker, Electrical conductivity of ferromagnetic compounds of manganese with perovskite structure, *Physica* **16**, 599 (1950).
[13]S. Jin, T. H. Tiefel, M. McCormack, R. A. Fastnacht, R. Ramesh and L. H. Chen, Thousandfold change in resistivity in magnetoresistive La-Ca-Mn-O Films, *Science* **264**, 413 (1994).
[14]J. B. Goodenough, An interpretation of the magnetic properties of the perovskite-type mixed crystals $La_{1-x}Sr_xCoO_{3-\lambda}$, *J. Chem. Phys. Solids* **6**, 287 (1958).
[15]C. S. Naiman, R. Gilmore, B. DiBartolo, A. Linz and R. Santoro, Lanthanum rhodium and lanthanum cobalt oxides *J. Appl. Phys*. **36**, 1044 (1965).
[16]P. M. Raccah and J. B. Goodenough, First-order localized-electron collective-electron transition in $LaCoO_3$, *Phys. Rev*. **155**, 932 (1967).
[17]V. G. Bhide, D. S. Rajoria, G. R. Rao and C. N. R. Rao, Mössbauer studies of the high-spin-low-spin equilibria and the localized-collective electron transition in $LaCoO_3$, *Phys. Rev. B* **6**, 1021 (1972).
[18]M. A. Korotin, S. Yu. Ezhov, I. V. Solovyev, V. I. Anisimov, D. I. Khomskii and G. A. Sawatzky, Electronic and spin configurations of Co^{3+} and Ni^{3+} ions in oxides of K_2NiF_4 structure: A magnetic susceptibility study, *Phys. Rev. B* **54**, 5309 (1996).
[19]M. M. Natile, E. Ugel, C. Maccato and A. Glisenti, $LaCoO_3$: Effect of synthesis conditions on properties and reactivity, *Appl. Catal. B* **72**, 351 (2007).
[20]W. C. Koehler and E. O. Wollan, Neutron-diffraction study of the magnetic properties of perovskite-like compounds $LaBO_3$, *J. Phys. Chem. Solids* **2**, 100 (1957).
[21]J. W. Seo, E. E. Fullerton, F. Nolting, A. Scholl, J. Fompeyrine and J. P. Locquet, Antiferromagnetic LaFeO3 thin films and their effect on exchange bias, *J. Phys. Condens. Matter* **20**, 264014 (2008).
[22]S. Acharya, J. Mondal, S. Ghosh, S. K. Roy and P. K. Chakrabarti, Multiferroic behavior of lanthanum orthoferrite ($LaFeO_3$), *Mater. Lett*. **64**, 415 (2010).
[23]S. Phokha, S. Pinitsoontorn, S. Maensiri and S. Rujirawat, Structure, optical and magnetic properties of $LaFeO_3$ nanoparticles prepared by polymerized complex method*, J. Sol-Gel Sci. Technol*. **71**, 333 (2014).
[24]A. Mitra, A. S. Mahapatra, A. Mallick, A. Shaw, M. Ghosh and P. K. Chakrabarti, Simultaneous enhancement of magnetic and ferroelectric properties of $LaFeO_3$ by co-doping with Dy^{3+} and Ti^{4+}, *J. Alloy. Comp*. **726**, 1195 (2017).

[25]H.-R. Fuh, K.-C. Weng, Y.-P. Liu and Y.-K. Wang, New ferromagnetic semiconductor double perovskites: La_2FeMO_6 (M = Co, Rh, and Ir), *J. Alloy. Comp*. **622**, 657 (2015).
[26]H.-R. Fuh, K.-C. Weng, C.-R. Chang and Y.-K. Wang, Electronic structure of ferromagnetic semiconductor material on the monoclinic and rhombohedral ordered double perovskites La_2FeCoO_6, *J. Appl. Phys*. **117**, 17B902 (2015).
[27]P. M. Tirmali, D. K. Mishra, B. P. Benglorkar, S. M. Mane, S. L. Kadam and S. B. Kulkarni, Structural, magnetic and dielectric relaxation behaviour study of La_2MnCoO_6 and fully substituted B-site La_2FeCoO_6, *J. Chin. Adv. Mater. Soc*. **6**, 207 (2018).
[28]K. M. Ginell, C. Horn, R. B. Von Dreele and B. H. Toby, Materials for learning use of GSAS-II, *Powder Diffr*. **34**, 184 (2019).
[29]B. H. Toby, EXPGUI, a graphical user interface for GSAS, *J. Appl. Cryst.* **34**, 210 (2001).
[30]C. E. Alarcón-Suesca, C. E. Deluque Toro, A. V. Gil Rebaza, D. A. Landínez Téllez and J. Roa-Rojas, Ab-initio studies of electronic, structural and thermophysical properties of the Sr_2TiMoO_6 double perovskite, *J. Alloys Compd*. **771**, 1080 (2019).
[31]B. D. Cullity, *Elements of X-ray Diffraction*, 2nd edn. (Addison Wesley Publishing Company, Reading, MA, 1978).
[32]M. Saleem, L. Fang, H. B. Ruan, F. Wu, Q. L. Huang, C. L. Xu and C. Y. Kong, Effect of zinc acetate concentration on the structural and optical properties of ZnO thin films deposited by Sol-Gel method, *Int. J. Phys. Sci*. **7**, 2971 (2012).
[33]B. R. Kumar and B. Hymavathi, X-ray peak profile analysis of solid-state sintered alumina doped zinc oxide ceramics by Williamson–Hall and size-strain plot methods*, J. Asian Ceram. Soc*. **5**, 94 (2017).
[34]E. Parthé, L. Gelato, B. Chabot, M. Penzo, K. Cenzual and R. Gladyshevskii, TYPIX Standardized and crystal chemical characterization of inorganic structure types, in *Gmelein Handbook of Inorganic and Organometallic Chemistry*, 8th edn. (Springer, Berlin, 1993).
[35]W. Wondratschek, Special topics on space groups, in *International Tables for Crystallography*, Vol. A, Chap. 8.3 (International Union of Crystallography 2006), p. 732.
[36]A. M. Glazer, The classification of tilted octahedra in perovskites, *Acta Cryst*. *B* **28**, 3384 (1972).
[37]C. A. Schneider, W. S. Rasband and K. W. Eliceiri, NIH image to ImageJ: 25 years of image analysis, *Nat. Meth.* **9**, 671 (2012).
[38]E. C. Aguiar, M. A. Ramirez, J. A. Cortes, L. S. Rocha, E. Borsaria and A. Z. Simões, Magnetoelectric coupling of $LaFeO_3$/$BiFeO_3$ heterostructures, *Ceram. Int*. **41**, 13126 (2015).
[39]Q. Yao, Ch. Tian, J. Wang, H. Zhou and G. Rao, Antiferromagnetic-ferromagnetic transition in Bi-doped $LaFeO_3$ nanocrystalline ceramics, *Ceram. Int.* **46**, 20472 (2020).
[40]H. Weihe and H. U. Güdel, Quantitative interpretation of the Goodenough-Kanamori rules: A critical analysis, *Inorg. Chem*. **36**, 3632 (1997).
[41]S. M. Khetrea, H. V. Jadhav, P. N. Jagadale, S. R. Kulal and S. R. Bamane, Studies on electrical and dielectric properties of $LaFeO_3$, *Adv. Appl. Sci. Res*. **2**, 503 (2011).
[42]L. Sudheendra, M. Seikh, A. R. Raju, C. Narayana and C. N. R. Rao, Dielectric properties of rare earth cobaltates, LnCoO3 (Ln = La, Pr, Nd), across the spin-state transition, *Ferroelectrics*, **306**, 227 (2004).
[43]J. F. Felix, E. F. da Silva Jr, E. A. De Vasconcelos and W. M de Azevedo, Tailoring the electrical properties of ZnO/Polyaniline heterostructures for device applications, *J. Korean Phys. Soc.* **58**, 1256 (2011).
[44]J. A. Cuervo Farfán, C. E. Deluque Toro, C. A. Parra Vargas, D. A. Landínez Téllez and J. Roa-Rojas, Experimental and theoretical determination of physical properties of $Sm_2Bi_2Fe_4O_{12}$ ferromagnetic semiconductors, *J. Mater. Chem. C* **8**, 14925 (2020).
[45]A. Vojta, Q. Wen and D. R. Clarke, Influence of microstructural disorder on the current transport behavior of varistor ceramics, *Comput. Mater. Sci*. **6**, 51 (1996).
[46]R. K. Pandey, W. A. Stapleton and I. Sutanto, The effect of doping with some rare earth oxides on electrical features of ZnO, *IEEE J. Electron Dev. Soc*. **3**, 276 (2015).
[47]A. Jüngel, *Quasi-hydrodynamic Semiconductor Equations* (Springer Basel AG, 2001).